# Integration of a versatile bridge concept in a 34 GHz pulsed/CW EPR spectrometer

Alan Band,[1] Matthew P. Donohue,[1,2] Boris Epel,[3] Shraeya Madhu,[4] Veronika A. Szalai[1*]

[1]Center for Nanoscale Science and Technology, National Institute of Standards and Technology, Gaithersburg, MD 20899; [2]Maryland NanoCenter, University of Maryland, College Park, MD 20742; [3]Center for EPR Imaging *in Vivo* Physiology, University of Chicago Medical Center, Chicago, IL 60637; [4]Poolesville High School, Poolesville, MD 20837

## Abstract

We present a 34 GHz continuous wave (CW)/pulsed electron paramagnetic resonance (EPR) spectrometer capable of pulse-shaping that is based on a versatile microwave bridge design. The bridge radio frequency (RF)-in/RF-out design (500 MHz to 1 GHz input/output passband, 500 MHz instantaneous input/output bandwidth) creates a flexible platform with which to compare a variety of excitation and detection methods utilizing commercially available equipment external to the bridge. We use three sources of RF input to implement typical functions associated with CW and pulse EPR spectroscopic measurements. The bridge output is processed via high speed digitizer and an in-phase/quadrature (I/Q) demodulator for pulsed work or sent to a wideband, high dynamic range log detector for CW. Combining this bridge with additional commercial hardware and new acquisition and control electronics, we have designed and constructed an adaptable EPR spectrometer that builds upon previous work in the literature and is functionally comparable to other available systems.

## Keywords

Electron paramagnetic resonance spectroscopy, EPR spectroscopy, DEER, arbitrary waveform generator, 34 GHz EPR spectrometer, pulsed EPR spectrometer, PELDOR, EPR instrumentation

## Introduction

The past sesquidecade has witnessed widespread applicability of pulse electron paramagnetic resonance (EPR) spectroscopy techniques [1] throughout scientific disciplines, from its founding realm of physics to the fields of chemistry, materials science, biology and medicine. Commercialization of spectrometers at multiple operating frequencies, in combination with pulse sequences designed to manipulate and extract information from spin systems, has produced a mature field where formerly esoteric, but now routine experiments can investigate the molecular dynamics of paramagnetic species. A new generation of experiments, however, exquisitely capable of manipulating spin systems with heretofore unrivaled excitation bandwidths, has been made possible by microwave pulse shaping technologies (for a recent review of pulse shaping in EPR spectroscopy, see Spindler *et al.*[2]). Arbitrary waveform generators (AWGs) equipped with nanosecond timing resolution, built onto existing commercial [3, 4] or custom-built spectrometers [5-10], have been used to demonstrate that pulse shaping in EPR spectroscopy presents several advantages over traditional experiments (i.e., those restricted to rectangular-like pulses).

Shaped microwave pulses, in which the carrier's phase, frequency or amplitude are arbitrarily modulated, and related instrumental requirements have recently found applications in several well-known EPR spectroscopy experiments. The double electron-electron resonance (DEER) experiment, for example, has benefitted from shaped pulses as demonstrated from increased modulation depths by pumping at larger, more selective bandwidths [11, 12]. The original four-pulse DEER sequence [13] itself has been newly modified for the inclusion of Carr-Purcell pulse trains [6, 14-16], for pre-polarization of high-spin systems [17] and also for the use of an entirely new dipolar pathway in the experiment [18]. Optimal control theory has been employed in Fourier Transform-EPR to account for the spectrometer response function [3]. Finally, three-dimensional

experiments, using ultra-wideband pulses to excite large hyperfine splittings, also have been demonstrated [19]. Most of these experiments were performed at either X-band (approximately 9.5 GHz) or Q-band[1] (34 GHz in the EPR community) operational frequencies.

The Q-band frequency is uniquely advantageous for measurements using the nitroxide radical, a common spin label/probe [20] used to investigate biomolecule dynamics in conjunction with EPR spectroscopy. In this frequency band, neither the Zeeman interaction nor the hyperfine interaction outright dominates the nitroxide spectrum so that an intermediate regime exists [21]. High-field EPR spectroscopy (frequencies at or above 95 GHz (W-band)) requires careful data analysis due to orientation selection effects, whereas at lower frequencies (X-band or lower) the spectrum narrows considerably, to the point of negligible *g*-anisotropy, so that care must be taken to avoid band overlap in dual-frequency experiments (e.g. DEER), necessitating a compromise in excitation bandwidths to collect spectra free from artifacts. For multi-frequency microwave experiments targeted towards elucidating hyperfine couplings (e.g. electron double resonance (ELDOR)-detected nuclear magnetic resonance (NMR)), the increase in the nuclear Zeeman frequency at Q-band, relative to X-band, aids in shifting signals away from the central hole of the spectrum [22, 23]. As a final example, pulsed EPR techniques used to detect low frequency hyperfine couplings, namely electron spin echo envelope modulation (ESEEM) and hyperfine sublevel correlation spectroscopy (HYSCORE), suffer from a reduction in modulation depths at higher frequencies, and the necessity of larger $B_1$ fields to excite forbidden transitions, but an advantage may be obtained through resolution of closely spaced multi-nuclear peaks. Additionally, in certain situations, the 'cancellation limit' is achieved at Q-band [24, 25], whereby

[1] Q band is not standardized, but common usage refers to a range of 33 GHz to 50 GHz. The EPR community generally refers to Q band as approximately 34 GHz.

maximum modulation depth is achieved. As such, Q-band offers several advantages over both X- and W-bands, and presents a desirable middle-ground to develop pulse shaping capabilities.

The goal of the work presented here was to create a fully-functional, combined pulsed/continuous wave EPR spectrometer intended for routine use in the National Institute of Standards & Technology's (NIST) Center for Nanoscale Science & Technology (CNST) user facility that integrates pulse shaping and operates at 34 GHz (Ka-band, which encompasses 26.5 GHz to 40 GHz per IEEE definitions [26]). Herein, we report a versatile design for a high-power 34 GHz spectrometer built using a custom commercial pulse/CW bridge architecture and outfitted with additional electronic components. The NIST spectrometer uses a commercial resonator designed for CW and pulsed experiments, with a relatively large active volume (3 mm outer diameter tubes) for sample access. Practical considerations, including the spectrometer design and performance, are presented and illustrate the feasibility and performance of the spectrometer system built with this approach.

## Instrument Design

Figure 1 shows the basic block diagram of our spectrometer system, with components used for CW (blue), pulsed mode (red), and both modes (purple). The component list is provided in Table 1.[2] For clarity, the block diagram specifically omits microwave switches (Tx Mute and Rx Mute) and bandpass filters in the up/down conversion stages in the bridge. Additional details on the bridge layout and architecture are in the Supporting Information (Figure S6).

[2]Certain commercial equipment, instruments, or materials are identified in this paper to specify the experimental procedure adequately. Such identification is not intended to imply recommendation or endorsement by the National Institute of Standards and Technology, nor is it intended to imply that the materials or equipment identified are necessarily the best available for the purpose.

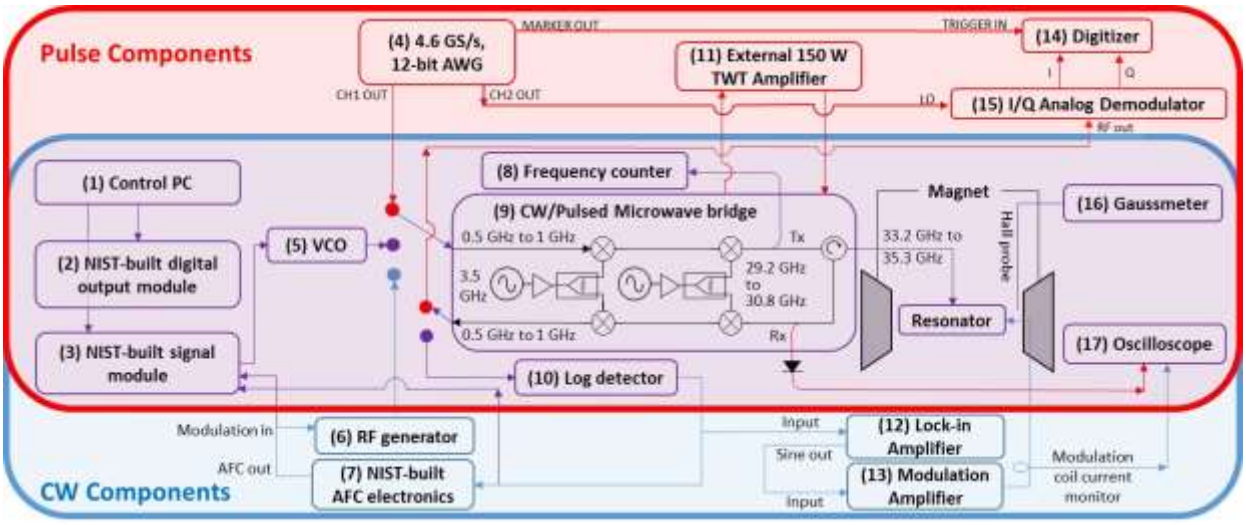


Figure 1: NIST Q-band EPR spectrometer block diagram. Components for CW (blue), pulsed (red) or both modes (purple) are shown. (1) Control PC running EPR spectrometer control software; (2) NIST-built digital output module to drive (external) switches for signal path selection and internal bridge switches; (3) NIST-built signal conditioning module for the multi-function PCIe board (see below); (4) AWG for direct RF excitation in pulse mode; (5) Voltage-controlled oscillator (VCO) for frequency sweeps during resonator tuning procedure; (6) Radiofrequency (RF) generator for RF input into bridge during CW operation; (7) NIST-built automatic frequency control (AFC) electronics for CW operation; (8) Frequency counter that measures upconverted frequency in the transmit path; (9) Bridge; (10) Logarithmic detector with 1 MHz to 4 GHz bandwidth, 80 dB dynamic range (11) External 150 W TWT amplifier for high power pulse experiments; (12) Lock-in amplifier providing 100 kHz modulation for CW operation; (13) Modulation amplifier with 20 dB gain, output voltage range of -40 V to +40 V; (14) Two channel digitizer with 8-bit resolution, 1.5 GHz bandwidth and sampling rate of 2 x $10^9$ $s^{-1}$ (simultaneous); (15) I/Q Demodulator with 400 MHz to 6 GHz range and local oscillator (LO) pulse provided by AWG Ch2; (16) Gaussmeter and Hall probe; (17) Oscilloscope to display modulation amplitude (as mA peak-to-peak) during CW operation or resonator ring down time via external diode detector connected to diagnostic receiver (Rx) path coupler (not shown). Other items not shown: the 10 MHz clock to which the internal bridge sources (3.5 GHz; 14.6 GHz to 15.4 GHz), RF generator, and sampling clock generator are synchronized; Rx mute & Tx mute switches; internal 10 W SSPA, and built-in Tx and Rx power monitors.

The highlight of our system is the versatile bridge design (Figure S6) loosely based on modern radar bridges that was proposed and built by Smiths Interconnect (formerly Millitech), expert in microwave engineering, under contract to the US Government. Adoption of this bridge layout impacted our overall instrument architecture and guided our procurement of the external

components required to create a fully-functioning EPR spectrometer system. Additional NIST-built electronics completed the system; details of select function modules of the hardware are provided in the SI. The most notable consequence of the bridge design is that we use three separate external sources of radiofrequency (RF) excitation, a voltage-controlled oscillator (VCO), an RF generator, and an AWG, to carry out resonator tuning (VCO), CW (RF generator) and pulsed mode (AWG) operation. The output frequency of the bridge ranges from 33.2 GHz to 35.3 GHz with an instantaneous bandwidth of 500 MHz. When the resonator bandwidth exceeds 500 MHz, or when an AWG is used to pre-distort pulses to compensate for limited resonator bandwidth, the 500 MHz bandwidth of the bridge can be limiting. The actual bridge operating frequency is determined by the sum of the bridge RF input frequency (500 MHz to 1 GHz), a first-stage upconverter local oscillator (LO) fixed at 3.5 GHz, and the second, programmable upconverter synthesizer frequency settable over a 29.2 GHz to 30.8 GHz range in 20 MHz steps. A careful accounting of these numbers verifies the stated 33.2 GHz to 35.3 GHz operating range of the bridge: 500 MHz + 3.5 GHz + 29.2 GHz = 33.2 GHz; 1 GHz + 3.5 GHz + 30.8 GHz = 35.3 GHz. There are three excitation paths available within the bridge: low power CW, pulse mode with an internal 10 W solid state power amplifier (SSPA), and pulse mode using an external 150 W traveling wave tube (TWT) amplifier. The TWT amplifier was built and tested to our specifications to have WR-28 waveguide in/out along with pre-shipment testing over our operating range of 33.2 to 35.2 GHz Motorized waveguide switches inside the bridge direct the transmit path to the software-selected amplifier. The bridge has waveguide connections allowing use of any reflection-based resonator either home-built or from commercial suppliers. The receive path gain (typically 31.25 dB) in the bridge is frequency-dependent and varies from 29 dB to 34 dB over the usable frequency range. Addition of the 150 W TWT amplifier necessitated use of a robust protection switch [27], with a peak power

rating of 200 W, to protect the low noise amplifier (LNA) in the receive path. The RF switch isolation was specified at 65 dB over the operating band; we measured 82 dB at 34.25 GHz. The pulsed and CW modes are distinguished principally by the excitation source and detection method used. A voltage-controlled oscillator (VCO) sweeps the frequency over a maximum range of 500 MHz for tuning to the resonator's resonant frequency, resulting in the intuitive power *vs* frequency scan displayed by the control software. This traditional tuning method was chosen for its simplicity although it has been demonstrated that an AWG chirp pulse (i.e. a pulse solely modulated using a linear frequency sweep) response could be used for this function [8]. The resonator's calculated resonant frequency is marked in software, and then measured using a frequency counter in the transmit (Tx) path of the bridge. Software then calculates the frequency setting for the bridge synthesizer and RF generator for CW operation and, in pulse mode, the AWG.

The main benefit of the NIST spectrometer is that the bridge is a commercial transceiver with IF in/out in the 0.5 GHz to 1 GHz range, which allows for customization and experimentation with the excitation/detection scheme. It permits a wide-variety of user-defined equipment to generate excitation signals (VCO, RF Generator, commercial AWG) and process the bridge output RF signal (detectors, demodulators, digitizers) without change to the microwave bridge. As an example, we performed an exercise to detect a Hahn echo of coal using a CW RF generator at the bridge input and formed rectangular-shaped pulses using a microwave switch in the bridge (Tx Mute, Figure S6), which allowed us to use our bridge like more conventional bridges that employ pulse-switches to generate microwave pulses. The echo was detected by attenuating and phase shifting the RF Generator output to provide the demodulator LO signal. After we had all parts on hand, the entire experiment (re-configuration, measurement, restoration to normal configuration) only took 2 h and did not require any software changes.

**Table 1: Key components of NIST Q-band EPR spectrometer**[2]

| Component name | Details |
|---|---|
| 10 MHz clock | Stanford FS725 Benchtop Rubidium Frequency Standard & Stanford FS735/1/1/ two 7-channel 10 MHz distribution amplifiers |
| Digitizer | Agilent Acqiris U1084A-001, sampling rate of $2 \times 10^9$ $s^{-1}$ - 2CH, sampling rate of $4 \times 10^9$ $s^{-1}$ -1CH |
| AWG | Keysight 81180B, sampling rate of $4.6 \times 10^9$ $s^{-1}$ 12-bit, 2 analog outputs, 4 marker outputs |
| VCO | Minicircuits ZX95-1300+ |
| Log detector | Analog devices ADL5513, 80 dB dynamic range |
| 150 W TWT Amplifier | Applied Systems Engineering 187ka, 34 GHz to 36 GHz |
| Frequency Counter | Anritsu MF2414C |
| CW/Pulsed microwave bridge | Smiths Interconnect (formerly Millitech) CW/pulsed EPR bridge, 33.2 GHz to 35.3 GHz |
| Resonator | Bruker QT-IIw |
| Lock-in amplifier | Stanford SR830 |
| Modulation amplifier | Accel TS200-5B |
| I/Q Demodulator | Signal Core SC5313A |
| RF signal generator | Stanford SG382 |
| Low noise amplifier | East Coat Microwave/Low Noise Factory LNF-LNR22_40WA |
| 4 GHz AWG – 2 GHz Digitizer Sampling Clock Generator | Chase Scientific CG6000 + Omni-Spectra XMAPD10-2-8-2S Power Divider + Pulse Research Labs PRL752-2 10GHz Frequency Divide-By-2 module |

*CW operation*

We implemented basic CW EPR capability that is primarily used to facilitate pulsed EPR experiment setup. Our approach uses conventional $B_0$ field modulation and detection of the modulation signal using a wide-dynamic range logarithmic envelope detector connected to the bridge RF output. We exclusively observe the traditional, familiar EPR absorption component by lock-in signal processing. It is necessary, however, to implement automatic frequency control (AFC) to suppress signal distortion due to the dispersion component which manifests as a shift in cavity resonance as the $B_0$ field is swept through EPR resonance. The AFC follows this frequency shift, thereby nulling dispersion related signal changes that would otherwise occur. Initially, we wanted to use the AWG as the RF source for both pulsed and CW experiments. AFC requires

externally driven frequency modulation of the RF carrier, a function which is not generally available in high speed ($> 2 \times 10^9$ $s^{-1}$) AWGs. Thus, the RF input for CW was shifted to an RF generator operating in the desired baseband frequency range (0.5 GHz to 1 GHz), which accepts a modulating signal from the NIST-built AFC circuit. After the resonator tuning procedure is completed, the spectrometer software control program shifts the required frequency to the RF generator for input into the bridge. One of the key features of the RF generator we selected is its wide frequency modulation (FM) mode frequency deviation, which is ± 8 MHz over our operating band. This feature allows our AFC to track cavity drifts over an extended range during CW data collection without the need for resetting the AFC.

Classically, a biased diode extracts the envelope of the lock-in signal directly from the reflected signal at microwave frequencies. Our system uses a logarithmic detector (1 MHz to 4 GHz, 80 dB input range, connected to the 500 MHz to 1 GHz bridge RF output) that provides a linear in dB voltage proportional to the bridge output power level. The output voltage follows reflected power variations as the frequency is swept during cavity tuning and detects both the 100 kHz, field-modulated EPR signal and the 10 kHz-modulated AFC signals during CW EPR measurements. In other words, this wide bandwidth (1 MHz to 4 GHz), high dynamic range (80 dB) logarithmic detector can singly perform signal processing for cavity tuning (log detector output DC coupled) as well as CW lock-in and AFC lock-in detection (log detector output AC coupled in these latter two cases). Without a diode in the CW receiver path, the need for a sophisticated reference arm to bias the detector into its linear region of operation is technically eliminated in our system. Note that our log detector's calibration is not affected by the specific power level being used if the power level is within its specified 0.1 nW to 0.01 W (-70 dBm to + 10 dBm) operating range. We typically run in the range of 10 nW to 1 μW (-50 dBm to -30 dBm) during CW operation. Although the

logarithmic detector's output is linear in dB by design, it is also quite linear over the typical small signal ranges (< 1dB variation) observed during CW experiments and produces very reasonable lineshapes without additional signal processing.

*Pulsed-mode operation*

For pulse mode, a single 12-bit digital-to-analog channel on the AWG provided all RF excitation at a sampling rate of $4 \times 10^9$ $s^{-1}$, resulting in a time resolution of 250 ps. Acquisition uses the 2nd AWG analog out channel to provide a phase-coherent LO pulse for the analog I/Q demodulator. The LO pulse length exceeds the time of the acquired record length of the expected signal and has an initial phase referenced to the initial time ($t_0$) of the sequence. The demodulator we use is a small, computer-controlled signal processing system that contains computer settable RF and LO filters, input RF amplifiers, input attenuators, and I/Q channel balance digital-to-analog converters (DACs) that have been set to initial values for correct I/Q channel signal amplitudes. These parameters are adjustable in software if further tuning is needed. Each of the I and Q demodulator output channels has a 3 dB bandwidth of 160 MHz, resulting in an instantaneous detection bandwidth of 320 MHz. To minimize timing jitter, we provide external sampling clock signals to both the AWG ($4 \times 10^9$ $s^{-1)}$ and the digitizer ($2 \times 10^9$ $s^{-1}$). This configuration resulted in AWG to digitizer sampling clock jitter on the order of 10 ps. Use of the I/Q demodulator sufficiently reduces signal bandwidth such that sampling each channel at $500 \times 10^6$ $s^{-1}$ (2 ns/point) is more than adequate. The digitizer board and software driver automatically perform sample decimation if the requested sample rate is lower than the actual conversion rate.

## Software control

For our spectrometer system, we use Specman4EPR commercially-available control software [28], which can be easily reconfigured to run a variety of EPR instruments. In our case, additional functionality (AWG engine to produce direct RF pulses, all functions for running CW experiments) was added to allow for use of this software in our instrument. For stand-alone devices, the software utilizes GPIB, USB and Ethernet hardware interfaces. A National Instruments PCIe-6351, NI X-series multi-function board generates digital output control signals, analog output control signals and digitizes low speed analog input signals. Every parameter or setting of the instrument can be changed as a part of an experiment, providing flexibility in experiment design.

The AWG engine in this control software uses pulse programming language (PPL) scripts to represent microwave pulses, delays and detection triggers. Although the hardware aspect of using AWGs is relatively straightforward, design of the user interface requires consideration of many factors because AWG pulse patterns are multi-parametric and should be calculated both inside and outside of the software. In the software, the simplicity of earlier developed PPL scripts is preserved to achieve the desired flexibility of control without compromising the program's performance.

The software provides spectrometer tuning interfaces that control CW and pulse acquisition modes. The additional interfaces include a resonator $S_{11}$ reflected power monitor with frequency sweep for resonator tuning and quality factor estimation. This plugin allows the user to mark the resonator frequency and zoom in on the resonator reflected power "dip". Another interface controls switching between spectrometer modes and excitation source. It measures output frequency using a microwave frequency counter and transfers this resonator frequency to the selectable input source (RF generator or AWG). It also controls the AFC circuit. Another useful

feature implemented in the software is a modified version of the "transient decay" or "decrement method" used to determine resonator Q factor [29, 30]. Manuals for commercial pulsed-EPR systems also describe this method [31]. In our software, timings are adjusted so that we observe a low-power reflected pulse, the shape of which is used to qualitatively determine resonator over- vs under-coupling and Q factor. Currently, we use hardware-demodulated (described above) signal detection in our system, but the software supports both hardware- and software-demodulated detection.

## Results

All chemicals were purchased from commercial suppliers and used without further purification. All pulsed EPR measurements were performed using an over-coupled commercial resonator with a maximum sample access of 3 mm and an active pulsed mode height of 16.5 mm. The TWT amplifier was used for all pulsed experiments. The spectrometer performance was experimentally verified with two routinely used and relatively complex pulse sequences, namely, the DEER experiment, designed to measure electronic dipolar interactions, and the electron spin echo envelope modulation (ESEEM) experiment, which measures nuclear hyperfine interactions. In addition, the signal to noise (*S/N*) performance of the spectrometer in pulsed mode operation was estimated from a primary echo obtained from a single shot (*vide infra*).

### *DEER Materials*

Polypeptide sequences are given in Table 2. These sequences have been demonstrated to fold as single, stable alpha helices in aqueous environments [32], affording a rigid biomolecular rod with which to attach spin labels.

**Table 2: Sequence of polyalanine peptides**

| Peptide name | Peptide sequence[a] |
|---|---|

| | |
|---|---|
| A5-26 | Ac-AAKAC(sl)AAKAAAAKAAAAKAAAAKAAC(sl)AKAY-$NH_2$ |
| A9-22 | Ac-AAKAAAAKC(sl)AAAKAAAAKAAAC(sl)KAAAAKAY-$NH_2$ |

[a]Ac-is an N-terminal acetyl group, -$NH_2$ is a C-terminal amide, and C(sl) are spin labeled cysteine residues

For the spin-labeling reaction, approximately 2.0 mg of crude peptide was dissolved in 1 mL deuterium oxide solution containing 10 mmol $L^{-1}$ tris(hydroxymethyl)aminomethane and 25 mmol $L^{-1}$ NaCl at pD = (7.62 ± 0.05) pH units (solvent P). The uncertainty on the pH value is based on the manufacturer's specification. The concentration of each polypeptide was determined by measuring its absorbance at 280 nm with the reported value of the extinction coefficient of L-tyrosine[33]. To each peptide solution, 2.1 mole equivalents of the spin label (*S*-(1-oxyl-2,2,5,5-tetramethyl-2,5-dihydro-1H-pyrrol-3-yl)methylmethanesulfonothioate) (MTSL) in acetonitrile were added. The reaction vessel was wrapped in foil to prevent unwanted photochemical reactions, and the solution was mixed on a tube rotator at room temperature for three hours. Excess MTSL was removed by three rounds of sequential concentration and dilution with solvent P using centrifugal concentrators. Concentrators with a nominal molecular weight limit of 3 000 Da were used. Following purification, supernatants were diluted with 500 µL solvent P containing 555 mg d8-glycerol (solvent G). The glycerol serves to promote vitrification, which lowers the potential for peptide aggregation. To determine the spin concentration, the samples were then drawn, by capillary action, into calibrated 10 µL disposable borosilicate glass micropipettes, sealed with a hematocrit tube sealing putty, and subsequently inserted into a commercial cylindrical $TE_{011}$ EPR cavity at room temperature for acquisition of continuous wave spectra at X-band on a commercial spectrometer. The integrated absorption intensities of the samples, normalized by their respectively measured loaded cavity quality factors ($Q_L$), were plotted against those of 4-hydroxy-2,2,6,6-tetramethylpiperidin-1-oxyl (TEMPOL) solutions of known concentrations as determined from visible absorption spectroscopy [34]. These TEMPOL solutions also were used for CW

performance testing. The solutions containing each spin-labeled polyalanine peptide were diluted with solvent G to a spin concentration of 500 μmol $L^{-1}$, and stored at -80 °C.

*DEER Performance*

All experiments were conducted at 70 K, and temperature stabilization within a continuous flow cryostat was controlled by a commercial temperature controller. The dead-time free, four pulse DEER sequence [13], using an eight step phase cycle on the first two pulses as described in Tait & Stoll [16] and outlined in Table 3, was employed for all measurements. The refocused echo generated after a time delay of $2\tau_1 + 2\tau_2$ from the center of the first pulse was integrated over the full width at about 1/3 height and taken as the signal. Due to limited resonator bandwidth, the observation frequency was set 40 MHz higher than the resonant frequency of the resonator ($\nu_{reson}$), while the pump frequency was set 40 MHz lower than $\nu_{reson}$ (see Figure 2 for resonator profile and the relative observe/pump frequency offsets).

**Table 3: Phase cycle used for the four pulse DEER sequence**

| $\varphi_1$ (°)* | $\varphi_2$ (°)* | In-phase channel detection coefficient | Quadrature channel detection coefficient |
|---|---|---|---|
| 0 | 0 | +1 | -i |
| 0 | 180 | +1 | -i |
| 180 | 0 | -1 | +i |
| 180 | 180 | -1 | +i |
| 90 | 0 | +i | +1 |
| 90 | 180 | +i | +1 |
| 270 | 0 | -i | -1 |
| 270 | 180 | -i | -1 |

*Phases are relative to the reference pulse

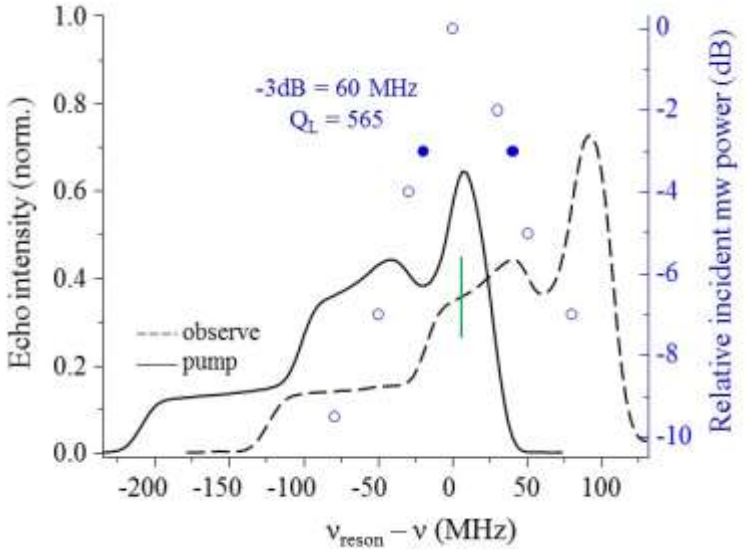


Figure 2: Right ordinate: open blue circles, depicting the resonator profile, indicate the microwave (mw) power required to maximize the primary electron spin echo signal, while staying on resonance with the central line ($m_I = 0$) of the nitroxide spectrum. The primary spin echo was generated using two rectangular-shaped $2\pi/3$ pulses [35], each 40 ns in duration, at 70 K. The filled blue circles report the – 3 dB points, which were used to calculate [36] the loaded Q factor ($Q_L$) = 565. Left ordinate: Echo-detected field sweeps of the A5-26 sample, converted to a frequency axis for comparison to the resonator profile, at the pump (solid black line) and observe (dashed black line) frequencies. Spectra are normalized relative to the maximum amplitude of the $m_I$ = +1 (low field) line taken at $\nu_{reson}$. The green line marks the on-resonance spin packets excited by the pump/observer center frequencies during the DEER experiment.

All pulses at the observer frequency were rectangular-shaped. The pulse issued at the pump frequency was either rectangular-shaped, or a sech amplitude modulated tanh frequency modulated [37] (sech/tanh) pulse, recognized as a highly selective broadband pulse.[38] A sech/tanh pulse can be described by its amplitude ($\nu_1(t)$) and frequency ($f_{mw}(t)$) modulation functions:

$$\nu_1(t) = \nu_1^{max}\, sech(\beta t) \tag{1}$$

$$f_{mw}(t) = f_c + \Delta f \frac{tanh(\beta t)}{2\, tanh\left(\beta/2\right)} \tag{2}$$

where $\nu_1^{max}$ is the maximum value of $\nu_1$, $\beta$ is the waveform truncation parameter, $f_c$ is the center frequency, $\Delta f$ is the difference between the end and start frequencies of the sweep and the time variable for a given pulse length, $T_p$, is $t \in \left[-T_p/2, T_p/2\right]$.

Over its duration, the sech/tanh pulse will invert spins sequentially as the instantaneous frequency ($f_{mw}(t)$) comes into resonance with Larmor frequencies of spin packets over the spectral bandwidth of interest. Sequential inversion may result in superposition of start times for dipolar evolution[15]; consequently, the pulse duration should be kept as short as possible, on the order of one quarter of the dipolar oscillation period [39], while also maintaining a high adiabaticity factor. For our peptide samples, the former restriction was addressed by setting the pulse duration to 100 ns, and the latter was met by using the maximum available power (main attenuator set to 0 dB) to achieve a high field strength ($\omega_1$) of the pulse. The remaining parameters for the sech/tanh pulse were empirically derived using the two point parameter $\eta_{2P} = V_0 - V_t$, as introduced by Doll *et al.*[17] for chirp pulses and used by Tait *et al.*[16] for sech/tanh pulses (Figure 3). With the offset frequency between pump and observe bands set at 80 MHz (see Figure 2), an upper limit was applied to the frequency sweep ($\Delta f$) of the pump pulse to mitigate band overlap. All shots were acquired at a 1 kHz repetition rate. The separation time between the first and second observer pulses was equal to twice the Larmor precession period of $^2H$ (254 ns). Electronic dipolar evolution functions and distributions of distances between the nitroxide moieties of the peptides are given in Figures 4 and 5. The extracted distribution functions are consistent with the expected distances between nitroxide moieties based on known geometrical constraints for an alpha-helical motif.

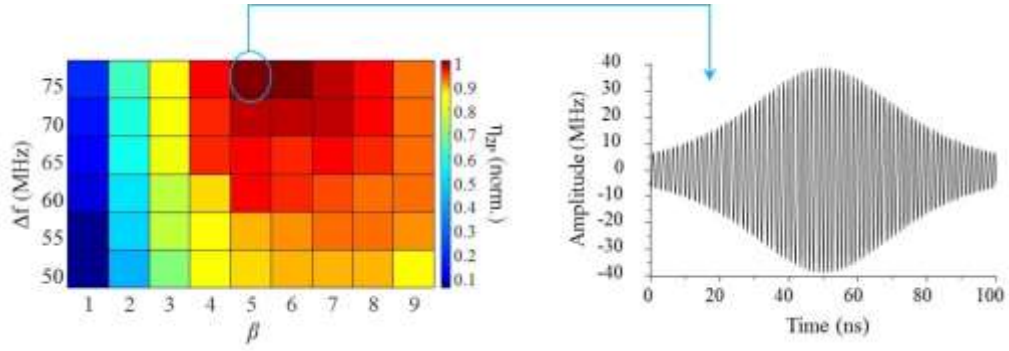

Figure 3: Left) *In situ* optimization of the amplitude truncation parameter ($\beta$) and the bandwidth of the frequency sweep ($\Delta$f) for the sech/tanh pump pulse in four-pulse DEER. The pulse duration was set to 100 ns and the frequency offset is displayed in Figure 1. $\eta_{2P}$ was recorded as the difference in the refocused echo amplitude when the pump pulse was issued at time zero ($V_0$, $t = 2\tau_1$) and at some later time ($V_t$, $t = 2\tau_1 + 200$ ns). At the maximum value of $\eta_{2P}$, $\beta = 5$ and $\Delta f = 75$ MHz, and these parameters were input into the sech/tanh pump pulse for both peptide samples. The A5-26 sample was used for this experiment. Right) Digital upconversion, using the LO of the AWG (at 750 MHz), of the optimized pulse.

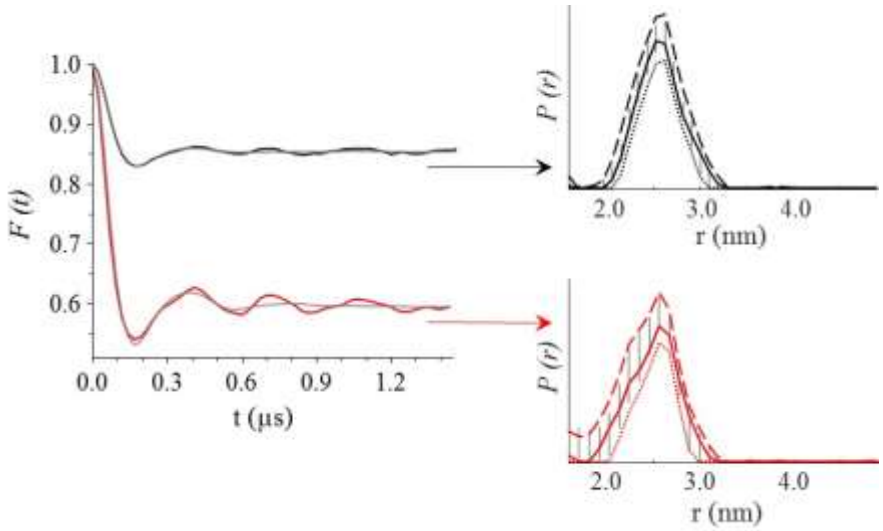


Figure 4: A9-22 sample - DEER time domain data and extracted distance distributions with error estimates, using either a 37-ns rectangular-shaped (black) or the optimized sech/tanh (red) pump pulse. Left) Validated form factors (*F(t)*). Grey curves, through application of Tikhonov regularization (TKR), represent simulated time domain signals (*S (t)*) computed from the optimum distance distribution (*P(r)*) (for a review of TKR, see [40, 41]). Right) Distance distributions. A series of form factors were generated for TKR, whereby all computations used a regularization parameter equal to 10. Combinatorial trials involving variation of the starting time for background division (the background is fit to an exponential decay within a set time interval), beginning at $t = 240$ ns and incrementing by 76 ns for 11 trials, and for 10 trials of artificial introduction of noise into the experimental data through pseudorandom number generation using a noise factor = 1.5, provided the series of form factors. Application of TKR to this series generated a population of 110 distance distributions. A lower error estimate corresponding to the mean value of the probability (‹r›) minus two times its standard deviation ($\sigma$) (dotted curve), an upper error estimate corresponding to ‹r› + 2$\sigma$ (dashed curve), and the optimum distribution with the lowest root mean square deviation (solid curve) of *S(t)* to *F(t)* are shown. Grey error bars indicate the full variation of the probability over all trials. Data analysis was performed using DeerAnalysis[42]. AWG programming and data acquisition transpired in 624 s (black) and 563 s (red).

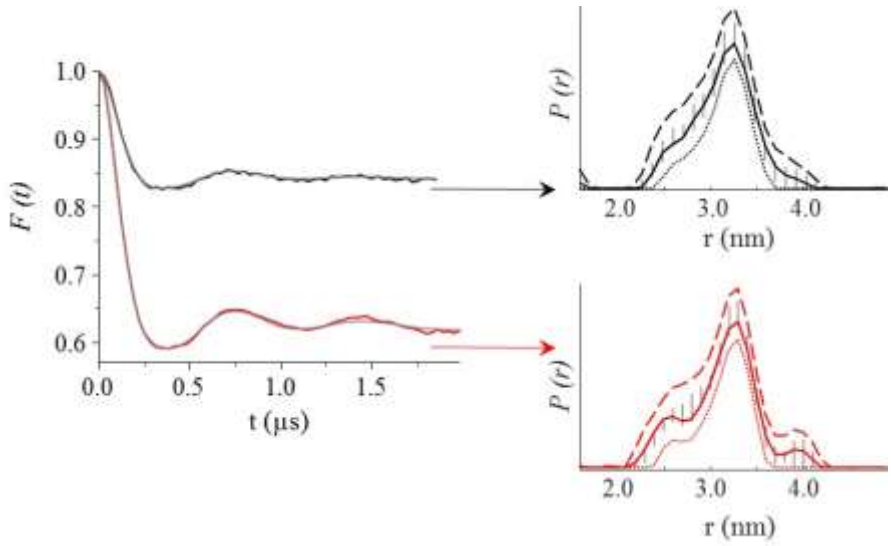


Figure 5: A5-26 sample - DEER time domain data and extracted distance distributions with error estimates, using either a 41-ns rectangular-shaped (black) or the optimized sech/tanh (red) pump pulse. Line-type descriptors are the same as those in Figure 5. AWG programming and data acquisition transpired in 659 s (black) and 994 s (red).

The mean time for signal averaging of the four DEER experiments shown in Figures 4 and 5 was just under 12 min, with markedly high *S*/*N* of the data sets. This timescale makes possible high throughput experiments, and is comparable to state-of-the-art instrumentation [18]. Using the program DeerAnalysis[42], amplitude modulation depths of the validated form factors were calculated to be approximately 0.40 for A9-22 and approximately 0.38 for A5-26 using the sech/tanh pump pulse. These modulation depths represent increases by factors of 2.6 relative to those calculated using the rectangular-shaped pump pulses. Further increases in modulation depth are to be expected by pumping with broader bandwidth sech/tanh pulses. This approach, however, demands a compromise in the observer refocused echo intensity as it must necessarily be shifted further from $\nu_{reson}$. Regarding the DEER experiment, the most significant experimental limitation of the NIST spectrometer currently is the bandwidth imposed by the resonator.

*CW Performance*

The CW capability of the spectrometer is demonstrated in Figure 6, displaying spectra of a set of serially-diluted aqueous TEMPOL solutions ranging in concentration from ≈ 795 μmol $L^{-1}$ to ≈ 50 μmol $L^{-1}$ (see the DEER Materials section) in 10 μL calibrated borosilicate micropipettes in the Bruker QT-II resonator at an incident microwave power of 15 μW. All spectra display the expected TEMPOL lineshape, and hyperfine splittings of approximately 1.7 mT (1.7 mT ± 0.1 mT in [43]). A CW spectrum of a 20 μmol $L^{-1}$ concentration TEMPOL sample was not detectable, but our sample volume was nearly 5-fold smaller than that provided by a standard Q-band capillary tube. The height of the CW active region of the resonator is 6.5 mm based on manufacturer information. Based on the 10 μL capillary tube dimensions, the volume of sample in the CW active region is ≈ 1.3 μL, which corresponds to ≈ $4 \times 10^{13}$ spins for the 50 μmol $L^{-1}$ TEMPOL sample. Detection of ≈ $4 \times 10^{13}$ spins is equivalent to detecting a 10 μmol $L^{-1}$ solution in a standard Q-band capillary (≈ 6.2 μL) in the same resonator.

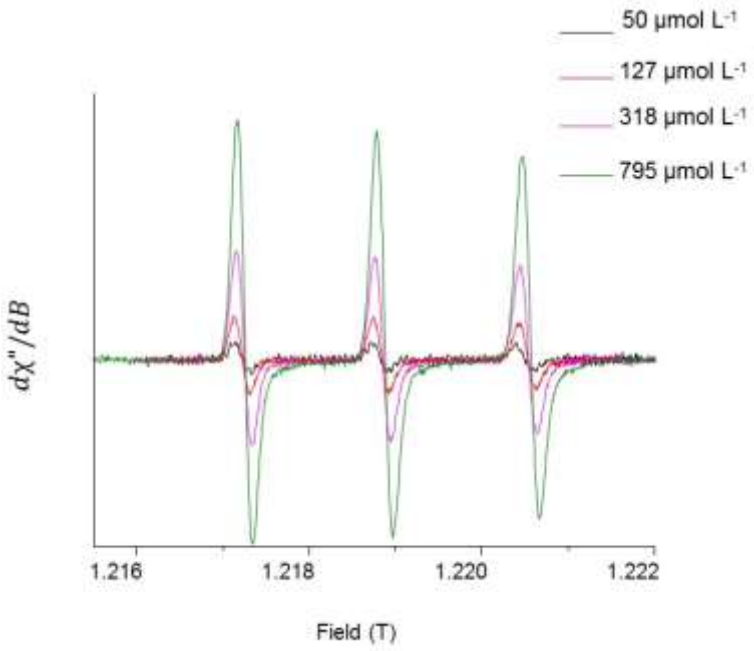


Figure 6: Room temperature CW EPR spectra of aqueous TEMPOL samples. Spectra colored green (≈ 795 μmol $L^{-1}$, average of 5 scans), magenta (≈ 318 μmol $L^{-1}$, average of 9 scans), red (≈ 127 μmol $L^{-1}$, average of 18 scans), and black (≈ 50 μmol $L^{-1}$, average of 24 scans) were

collected at 15 μW incident power, 0.2 mT modulation amplitude, 1024 points, 8 mT sweep width.

*Signal-to-Noise (S/N) Materials*

As a final performance test of the spectrometer, a rod of commercially-obtained clear, fused quartz ($SiO_2$) of (1.60 ± 0.013) mm outer diameter (diameter uncertainty is manufacturer specification) was irradiated by a $^{60}Co$ gamma-ray beam at NIST to a dose of (261 ± 2 %) Gy (dose uncertainty is based on manufacturer information). This sample type has been proposed as a spin echo standard by the Eaton group [44] because, as they have noted [45], its spin lattice relaxation time is long enough so that the echo may be conveniently observed at room temperature (see Figure 7 for relaxation data), and the echo signal is intense enough to be observed with a single shot while the noise is within the vertical resolution of the 8-bit digitizer. In addition, the *E'* center electrons of gamma irradiated quartz samples have reported mean lifetimes on the order of $1 \times 10^8$ years [46], rendering the sample quite stable after the date of irradiation. The sample was loaded into the resonator at room temperature (approximately 293 K) and occupied the full pulsed mode active volume. The resonator was maximally over-coupled to $Q_L$ of approximately 1095 (see Figure S7).

*Signal-to-Noise (S/N) Performance*

Single shot electron spin echoes generated from the quartz sample were recorded using two waveforms; hard monochromatic rectangular pulses, of 6 ns (π/2) and 12 ns (π) durations, were used to generate a Hahn echo, while sech/tanh pulses calibrated to compensate for the resonator bandwidth were used to generate the broadband echo. The calibration of the sech/tanh pulses is documented within the SI. Both echoes were recorded at the field position indicated in Figure 7,

at approximately the center of the absorption spectrum. The radical concentration in the 261 Gy sample, approximately $5.5 \times 10^{15}$ spins $cm^{-3}$, calculated using known concentrations of TEMPOL solutions loaded into calibrated 20 µL disposable borosilicate glass capillary (for determination of the spin concentration see the procedure outlined within the *DEER Materials* section), corresponded to approximately $1.7 \times 10^{14}$ spins excited by the broadband pulses. The TEMPOL calibration curve was constructed using an incident power of approximately 15 µW, corresponding to the regime in which the EPR signal is linear with respect to microwave power. In generating the TEMPOL calibration curve, we estimate the error of the visible absorption of TEMPOL to be less than 5 %, based on the manufacturer specifications for the instrument, and the error in the measured $Q_L$ for each sample is estimated to be 5 %, based on our observations of the fluctuation of the $Q_L$ value displayed in the software. Finally, the TEMPOL solutions and the quartz rod occupied inequivalent volumes within the X-band cavity; specifically, the column of an aqueous sample within a glass capillary extended approximately 380 µm away from the cavity center while the quartz rod extended outwards to approximately 800 µm from the center. However, to make our calculations, we assumed that differences in the $B_1$ field and modulation field distributions are negligible at sub-millimeter distances from the center of the cavity.

Following the approach taken in reference [47], the amplitudes of the in-phase components of both echo types, as measured with a cursor using open-access KAZAN Viewer software [48] were taken as the signal. The noise was determined from the standard deviation of the last 300 ns (500 ns to 800 ns; last 150 points) of each spectrum. The measurement bandwidth was limited to the demodulator's I/Q bandwidth of 160 MHz. The *S/N* of the Hahn echo was calculated to be approximately 32 and the *S/N* of the broadband echo was approximately 31 (see Figure 7 for echoes of the quartz sample). Although *S/N* comparisons were presented between three X-band

spectrometers and two laboratories in reference [44], the common critical component between those measurements was the resonator. For a direct comparison to be made from our measurements to those previously reported, a more rigorous characterization of the resonator, particularly of the filling factor, which contributes linearly to the signal voltage, would be needed.

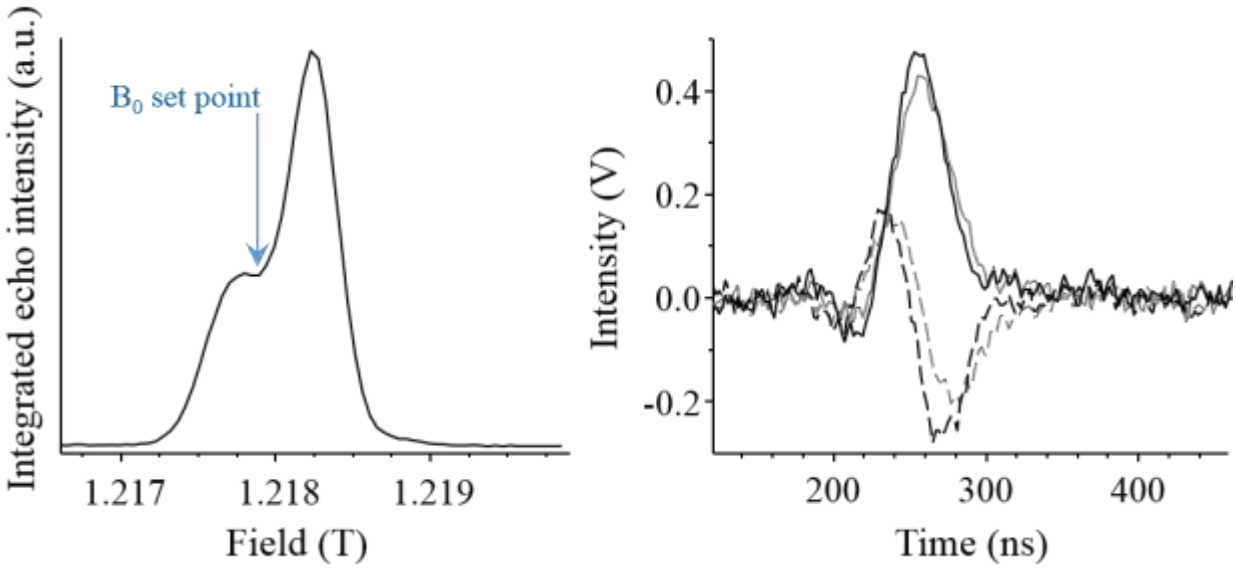


Figure 7: Left) Echo detected field sweep of the gamma irradiated quartz sample. The field position for the single shot primary echo experiment is indicated with a blue arrow. At room temperature, the longitudinal relaxation time ($T_1$) at the indicated field position was measured by inversion recovery and calculated to be ≈ 237 µs. Right) Hahn echo (grey) and broadband echo (black) generated from a single shot. The in-phase components are depicted as solid lines, while the quadrature components are dashed lines.

## Conclusions

The NIST CW/pulsed Q-band spectrometer uses a microwave bridge with RF-in/RF-out design (500 MHz to 1 GHz input/output passband), resulting in an instantaneous input/output bandwidth of 500 MHz, uses two stages of up/down conversion and custom bandpass filters to eliminate LO feedthrough. A mix of NIST-developed and commercially-available external (to bridge)

components were used to complete the spectrometer. Like other AWG-based EPR spectrometer designs, we eliminate the need for pulse forming networks, *viz* our rectangular pulse shapes do not depend upon the speed with which the classic "pulse-switch" turns on and off, nor do DEER experiments require a second, continuously running microwave source. Instead, the 500 MHz to 1 GHz input band permits one to choose off-the-shelf sources of excitation (AWGs, RF generators, etc.) to create custom pulses, pulse sequences, and CW excitation with external AFC. The bridge 500 MHz to 1 GHz output band also permits use of a wide variety of commercially-available detection devices (high speed digitizers, external demodulators, RF envelope detectors - logarithmic or linear), thereby creating custom EPR signal processing systems. All these modifications can be made without any changes to the microwave bridge itself. The spectrometer performance was demonstrated with DEER, ESEEM (not shown), and CW measurements. The *S/N* of a spin echo generated with a single shot using rectangular or broadband pulses produced *S/N* values of approximately 32 (rectangular) and approximately 31 (broadband). An AWG is used for baseband excitation in pulsed mode, and permits arbitrary amplitude, frequency and phase modulated pulses. We have demonstrated broadband spin excitation and inversion using sech/tanh pulses at 34 GHz with the inclusion of a 150 W amplifier within the spectrometer's excitation chain. Overall, we have successfully built a combined pulsed/continuous wave EPR spectrometer for routine use in the CNST user facility that integrates pulse shaping and operates at 34 GHz, allowing a wide variety of conventional and advanced pulsed EPR measurements to be performed. In so doing, our familiarity with the hardware design details will allow us to perform experiments many years into the future by either astute utilization or extension of our design.

**Acknowledgments**

We thank Marc Desrosiers at NIST for preparation of the γ-irradiated quartz tube used for initial signal-to-noise measurements. We thank Alexey Silakov, Peter Doan, George Cutsail, Raanan Carmieli, Mark Tseitlin, Andrei Astashkin, Ed Reijerse, Stefan Stoll, Ralph Weber, and Sergey Milikisiyants for assistance with many aspects of spectrometer development. Jared Greenberg and Chris Merola of Smiths Interconnect (formerly known as Millitech) are acknowledged for proposing and developing the microwave bridge architecture. Steve Blankenship & Dave Rutter are acknowledged for help with electronics and instrumentation design/building. Dr. Matthew Donohue acknowledges support under the Cooperative Research Agreement between the University of Maryland and the National Institute of Standards and Technology Center for Nanoscale Science and Technology, Award 70NANB10H193, through the University of Maryland. Shraeya Madhu thanks the Summer High School Intern Program at NIST. Boris Epel acknowledges NIH P41 EB002034 and R50 CA211408 grant support.

**Conflicts of interest**: none

## References


[1] A. Schweiger, G. Jeschke, Principles of Pulse Electron Paramagnetic Resonance, Oxford University Press, (2001).

[2] P.E. Spindler, P. Schöps, A.M. Bowen, B. Endeward, T.F. Prisner, Shaped Pulses in EPR, in: eMagRes, John Wiley & Sons, Ltd, 2016.

[3] P.E. Spindler, Y. Zhang, B. Endeward, N. Gershernzon, T.E. Skinner, S.J. Glaser, T.F. Prisner, Shaped optimal control pulses for increased excitation bandwidth in EPR, J. Magn. Reson., 218 (2012) 49-58.

[4] A. Doll, S. Pribitzer, R. Tschaggelar, G. Jeschke, Adiabatic and fast passage ultra-wideband inversion in pulsed EPR, J. Magn. Reson., 230 (2013) 27-39.

[5] T. Kaufmann, T.J. Keller, J.M. Franck, R.P. Barnes, S.J. Glaser, J.M. Martinis, S. Han, DAC-board based X-band EPR spectrometer with arbitrary waveform control, J. Magn. Reson., 235 (2013) 95-108.

[6] P.P. Borbat, E.R. Georgieva, J.H. Freed, Improved Sensitivity for Long-Distance Measurements in Biomolecules: Five-Pulse Double Electron–Electron Resonance, The Journal of Physical Chemistry Letters, 4 (2013) 170-175.

[7] Y.S. Yap, Y. Tabuchi, M. Negoro, A. Kagawa, M. Kitagawa, A Ku band pulsed electron paramagnetic resonance spectrometer using an arbitrary waveform generator for quantum control experiments at millikelvin temperatures, Review of Scientific Instruments, 86 (2015) 063110.

[8] M. Tseitlin, R.W. Quine, G.A. Rinard, S.S. Eaton, G.R. Eaton, Digital EPR with an arbitrary waveform generator and direct detection at the carrier frequency, J. Magn. Reson., 213 (2011) 119-125.

[9] D.K. Park, G. Feng, R. Rahimi, J. Baugh, R. Laflamme, Randomized benchmarking of quantum gates implemented by electron spin resonance, J. Magn. Reson., 267 (2016) 68-78.

[10] C.L. Motion, J.E. Lovett, S. Bell, S.L. Cassidy, P.A.S. Cruickshank, D.R. Bolton, R.I. Hunter, H. El Mkami, S. Van Doorslaer, G.M. Smith, DEER Sensitivity between Iron Centers and Nitroxides in Heme-Containing Proteins Improves Dramatically Using Broadband, High-Field EPR, The Journal of Physical Chemistry Letters, 7 (2016) 1411-1415.

[11] M.P. Donohue, V.A. Szalai, Distance measurements between paramagnetic ligands bound to parallel stranded guanine quadruplexes, Physical Chemistry Chemical Physics, 18 (2016) 15447-15455.

[12] C.L. Motion, S.L. Cassidy, P.A.S. Cruickshank, R.I. Hunter, D.R. Bolton, H. El Mkami, S. Van Doorslaer, J.E. Lovett, G.M. Smith, The use of composite pulses for improving DEER signal at 94 GHz, J. Magn. Reson., 278 (2017) 122-133.

[13] M. Pannier, S. Veit, A. Godt, G. Jeschke, H.W. Spiess, Dead-Time Free Measurement of Dipole–Dipole Interactions between Electron Spins, J. Magn. Reson., 142 (2000) 331-340.

[14] P.E. Spindler, I. Waclawska, B. Endeward, J. Plackmeyer, C. Ziegler, T.F. Prisner, Carr–Purcell Pulsed Electron Double Resonance with Shaped Inversion Pulses, The Journal of Physical Chemistry Letters, 6 (2015) 4331-4335.

[15] P.E. Spindler, S.J. Glaser, T.E. Skinner, T.F. Prisner, Broadband Inversion PELDOR Spectroscopy with Partially Adiabatic Shaped Pulses, Angewandte Chemie International Edition, 52 (2013) 3425-3429.

[16] C.E. Tait, S. Stoll, Coherent pump pulses in Double Electron Electron Resonance spectroscopy, Physical Chemistry Chemical Physics, 18 (2016) 18470-18485.

[17] A. Doll, M. Qi, N. Wili, S. Pribitzer, A. Godt, G. Jeschke, Gd(III)–Gd(III) distance measurements with chirp pump pulses, J. Magn. Reson., 259 (2015) 153-162.

[18] A. Doll, G. Jeschke, Double electron-electron resonance with multiple non-selective chirp refocusing, Physical Chemistry Chemical Physics, 19 (2017) 1039-1053.
[19] T.F. Segawa, A. Doll, S. Pribitzer, G. Jeschke, Copper ESEEM and HYSCORE through ultra-wideband chirp EPR spectroscopy, The Journal of Chemical Physics, 143 (2015) 044201.
[20] G.I. Likhtenshtein, J. Yamauchi, S. Nakatsuji, A.I. Smirnov, R. Tamura, Nitroxides: Applications in Chemistry, Biomedicine, and Materials Science, Wiley-VCH Verlag GmbH & Co. KGaA, (2008).
[21] Y. Polyhach, E. Bordignon, R. Tschaggelar, S. Gandra, A. Godt, G. Jeschke, High sensitivity and versatility of the DEER experiment on nitroxide radical pairs at Q-band frequencies, Physical Chemistry Chemical Physics, 14 (2012) 10762-10773.
[22] G. Jeschke, H.W. Spiess, NMR-correlated high-field electron paramagnetic resonance spectroscopy, Chemical Physics Letters, 293 (1998) 9-18.
[23] S. Van Doorslaer, E. Vinck, The strength of EPR and ENDOR techniques in revealing structure-function relationships in metalloproteins, Physical Chemistry Chemical Physics, 9 (2007) 4620-4638.
[24] G.J. Yeagle, M.L. Gilchrist, L.M. Walker, R.J. Debus, R.D. Britt, Multifrequency electron spin-echo envelope modulation studies of nitrogen ligation to the manganese cluster of photosystem II, Philosophical Transactions of the Royal Society B: Biological Sciences, 363 (2008) 1157-1166.
[25] T. Lohmiller, V. Krewald, M.P. Navarro, M. Retegan, L. Rapatskiy, M.M. Nowaczyk, A. Boussac, F. Neese, W. Lubitz, D.A. Pantazis, N. Cox, Structure, ligands and substrate coordination of the oxygen-evolving complex of photosystem II in the S2 state: a combined EPR and DFT study, Physical Chemistry Chemical Physics, 16 (2014) 11877-11892.
[26] 521-2002 - IEEE Standard Letter Designations for Radar-Frequency Bands, 2003, The Institute of Electrical and Electronics Engineers, Inc, New York, NY, http://ieeexplore.ieee.org/document/1160089/
[27] A.V. Astashkin, J.H. Enemark, A. Raitsimring, 26.5–40 GHz Ka-band pulsed EPR spectrometer, Concepts in Magnetic Resonance Part B: Magnetic Resonance Engineering, 29B (2006) 125-136.
[28] B. Epel, I. Gromov, S. Stoll, A. Schweiger, D. Goldfarb, Spectrometer manager: A versatile control software for pulse EPR spectrometers, Conc Magn Reson B, 26B (2005) 36-45.
[29] E.L. Ginzton, Microwave Measurements, McGraw-Hill Book Company, New York, NY, 1957.
[30] R.W. Quine, D.G. Mitchell, G.R. Eaton, A general purpose Q-measuring circuit using pulse ring-down, Concepts in Magnetic Resonance Part B: Magnetic Resonance Engineering, 39B (2011) 43-46.
[31] R.T. Weber, Pulsed EPR Primer, in: 23rd International EPR Symposium: 2nd pulsed EPR Workshop, Denver, CO, 2000, pp. 62.
[32] S. Marqusee, V.H. Robbins, R.L. Baldwin, Unusually stable helix formation in short alanine-based peptides, Proceedings of the National Academy of Sciences of the United States of America, 86 (1989) 5286-5290.
[33] H. Edelhoch, Spectroscopic Determination of Tryptophan and Tyrosine in Proteins, Biochemistry, 6 (1967) 1948-1954.
[34] R.G. Kooser, E. Kirchmann, T. Matkov, Measurements of spin concentration in electron paramagnetic resonance spectroscopy preparation of standard solutions from optical absorption, Concepts in Magnetic Resonance, 4 (1992) 145-152.

[35] E.L. Hahn, Spin Echoes, Physical Review, 80 (1950) 580-594.
[36] A. Raitsimring, A. Astashkin, J.H. Enemark, A. Blank, Y. Twig, Y. Song, T.J. Meade, Dielectric Resonator for K(a)-Band Pulsed EPR Measurements at Cryogenic Temperatures: Probehead Construction and Applications, Applied magnetic resonance, 42 (2012) 441-452.
[37] M.S. Silver, R.I. Joseph, D.I. Hoult, Highly selective π2 and π pulse generation, J. Magn. Reson., 59 (1969) 347-351.
[38] M. Garwood, L. DelaBarre, The Return of the Frequency Sweep: Designing Adiabatic Pulses for Contemporary NMR, J. Magn. Reson., 153 (2001) 155-177.
[39] A. Doll, M. Qi, A. Godt, G. Jeschke, CIDME: Short distances measured with long chirp pulses, J. Magn. Reson., 273 (2016) 73-82.
[40] G. Jeschke, G. Panek, A. Godt, A. Bender, H. Paulsen, Data analysis procedures for pulse ELDOR measurements of broad distance distributions, Applied Magnetic Resonance, 26 (2004) 223.
[41] Y.-W. Chiang, P.P. Borbat, J.H. Freed, The determination of pair distance distributions by pulsed ESR using Tikhonov regularization, J. Magn. Reson., 172 (2005) 279-295.
[42] G. Jeschke, V. Chechik, P. Ionita, A. Godt, H. Zimmermann, J. Banham, C.R. Timmel, D. Hilger, H. Jung, DeerAnalysis2006—a comprehensive software package for analyzing pulsed ELDOR data, Applied Magnetic Resonance, 30 (2006) 473-498.
[43] J.J. Windle, Hyperfine Coupling Constants for Nitroxide Spin Probes in Water and Carbon Tetracbloride, J. Magn. Reson., 45 (1981) 432-439.
[44] G.R. Eaton, S.S. Eaton, R.W. Quine, D. Mitchell, V. Kathirvelu, R.T. Weber, A Signal-to-Noise Standard for Pulsed EPR, J. Magn. Reson., 205 (2010) 109-113.
[45] S.S. Eaton, G.R. Eaton, Irradiated Fused-Quartz Standard Sample for Time-Domain EPR, Journal of Magnetic Resonance, Series A, 102 (1993) 354-356.
[46] P.-H. Huang, S.-Z. Jin, Z.-C. Peng, R.-Y. Liang, Y.-c. Quan, Z.-R. Wang, ESR dating and trapped electrons lifetime of quartz grains in loess of China, Quaternary Science Reviews, 7 (1988) 533-536.
[47] W.B. Mims, Envelope Modulation in Spin-Echo Experiments, Physical Review B, 5 (1972) 2409-2419.
[48] B.E. Epel, A. Silakov, Kazan Viewer Version 1.4.9: Visualization and data processing GUI for EPR and NMR, (2006).